Journal of Energy Storage 37 (2021) 102476

Contents lists available at ScienceDirect

Journal of Energy Storage

journal homepage: www.elsevier.com/locate/est

Electrochemical performance of potato-derived activated carbon: Effect of compressive stress

Yulin Zhang [a,1], Wei Sun [b,a,1], Fuqian Yang [a,*]

[a] Materials Program, Department of Chemical and Materials Engineering, University of Kentucky, Lexington, KY 40506, USA
[b] College of Chemistry, Chemical Engineering and Environmental Engineering, Liaoning Shihua University, Fushun, Liaoning, 113001, China

ARTICLE INFO

Keywords:
Biomass
Supercapacitor
Compressive stress
Specific capacitance
IR drop

ABSTRACT

The progress in smart electronics and photonics has imposed a great need for the development of portable, flexible devices and systems for energy storage from sustainable and eco-friendly resources. In this work, we synthesize porous activated carbon (AC) from potato mash via hydrothermal process and H_2O-steam activation and construct symmetrical supercapacitors with the potato-derived ACs as electrode material and 6 M KOH aqueous solution as electrolyte. The effects of the mass loading of the electrode material and compressive stress in a range of 1.69~6.92 MPa on the electrochemical performance of the supercapacitors are investigated. The experimental results reveal that increasing the compressive stress increases the specific capacitance of the supercapacitors and the diffusivity for ionic migration in the supercapacitors and causes the decreases of the IR drop, the series resistance and the intrinsic resistance. The method used in this work provides a feasible technique to increase the energy storage in supercapacitors.

1. Introduction

The rapid progress in smart electronics and photonics [1-5] has imposed a great need for the development of portable, flexible devices and systems for energy storage. There are two types of energy-storage devices and systems with great potential in the applications of smart electronics and photonics. One is metal-ion-based batteries, such as lithium-ion battery [6,7], which is based on the conversion between chemical energy and electrical energy; the other is electrochemical capacitors (supercapacitors) [8-10], which is based on electrical double layer, i.e. the accumulation of ions on solid surface, and/or redox pseudo-capacitance. The characteristics of fast-charging and potentially safer storage of energy for supercapacitors likely make them preferable choices in the applications of smart, portable-flexible devices and systems.

In general, smart, flexible electronics and photonics are continuously experiencing mechanical deformation, which can alter the performance of the energy devices and systems used to power the associated flexible electronics and photonics. Bu et al. [11] observed the drying-induced collapse of carbon nanocages, leading to simultaneous improvement of volumetric performance and increase of the energy density of the supercapacitors with electrode material from the collapsed carbon nanocages and electrolyte from inorganic electrolyte and ionic liquid. Using elastomeric electrospun separator and elastomeric electrodes, Li et al. [12] studied the effect of dynamic stretch and bending on the performance of supercapacitors with buckled single-walled carbon nanotube films. They did not observe significant variation in the performance of the supercapacitors under the stretch and bending. Applying different pressures in the extraction of Green Monoliths (GMs) of self-adhesive carbon grain and using the GM-derived activated carbon (AC) as electrode material, Awitdrus et al. [13] revealed the improvement of the electrochemical performance of the associated supercapacitors with the increase of the pressure used in the extraction of the carbon grains. Li et al. [14] demonstrated the increase of the specific capacitance of carbon-nanotube-based supercapacitors with increasing compressive stress. Using polypyrrole-mediated graphene foam as electrode materials for compressible supercapacitors, Zhao et al. [15] found that the compression has little effect on the specific capacitance of the supercapacitors for the compression strain up to 0.5. Using carbon-nanotube sponges as electrode of a supercapacitor, Li et al. [16] observed that the specific gravimetric capacitance of the supercapacitors under a 0.8 compressive strain was less than that without compression.

* Corresponding author.
E-mail addresses: fuqian.yang@uky.edu, fyang2@uky.edu (F. Yang).
[1] Equally contributing first author

https://doi.org/10.1016/j.est.2021.102476
Received 17 December 2020; Received in revised form 25 February 2021; Accepted 15 March 2021
Available online 23 March 2021

Chen et al. [17] constructed solid state supercapacitors with conductive, flexible polypyrrole as electrode materials and found that the bending, stretching and folding had little effect on the performance of the supercapacitors. Zhang et al. [18] showed that the supercapacitors with aerogels from nitrogen-doped graphene oxide and cellulose nanofibers exhibited good capacitive characteristic after 100 compressive-unloading cycles. Masarapu et al. [19] found that the increase of the specific gravimetric capacitance of flexible supercapacitors from nanostructured AC fibers with the increase of pressure consisted of two stages: one with small increase rates for small pressure, and the other with large increase rates for large pressure. Recently, Sun et al. [20] studied the effect of compressive stress on the electrochemical performance of the supercapacitors with xylose-derived AC spheres and Na_2SO_4 electrolyte and developed a power law relationship between the compressive stress and specific gravimetric capacitance. They found that the apparent diffusivity for ionic migration increased with the increase of the compressive stress.

According to the above discussion, it is evident that there likely exists mechanochemical interaction in supercapacitors during electrochemical cycling, controling the electrochemical performance of the supercapacitors. However, there are few studies focusing on the stress (pressure) effect on the supercapacitors made from biomass-derived activated carbon. Also, the effect of mechanical deformation on the performance of supercapacitors remains elusive.

It is known that potato is one of favorite foods world widely, and its production was more than 21.7 billion kg in 2011 [21]. However, significant amount of potato is wasted globally every year [22]. There is a great interest to use the potato waste to produce biofuel [21] and bioproducts for energy storage. Considering the need to manufacture devices and systems for the storage of renewable energy from sustainable and eco-friendly resources, we investigate the electrochemical performance of symmetric, two-electrode supercapacitors made from potato-derived ACs under concurrent action of compressive stress. The potato-derived AC, which is synthesized via hydrothermal carbonization and physical activation (H_2O steam) of potato mash, is used as electrode material. The study is focused on the dependence of the electrochemical performance of the supercapacitors on the thickness (mass loading) of electrode and compressive stress.

2. Experimental details

The potatoes purchased from local food market were boiled in water for 30 min and crushed to a mash. A mixture consisting of 30 g potato mash and 50 mL deionized water (DI water) was placed in a 100 mL Teflon liner under sonication for 20 min. The Teflon liner with the mixture was then put in a stainless-steel autoclave, which was tightly sealed and placed in an oven for hydrothermal carbonization of the mixture at 200 °C for 24 h. The solid product (biochar) collected from the Teflon liner after the hydrothermal carbonization was washed by DI water several times and then dried at 90 °C in an oven for 12 h. The product yield for the conversion of potato mash to biochar and ACs were ~16.2% and ~6%, respectively.

The dried biochar was physically activated at 800 °C for 1 h in a tube furnace. During the activation, there was continuous flow of nitrogen gas and H_2O steam with nitrogen gas as protective agent and H_2O steam as activation agent. The flow rate of nitrogen gas was 3 mm^3/s. The flow rate of water used to generate H_2O steam was 0.2 mm^3/s, and the H_2O steam was used for the activation of the potato-derived bichar. The solid powder (activated carbon) in the tube furnace after the physical activation was amassed and stored in an oven prior to being used in the construction of supercapacitors.

The microstructures of the solid powder (activated carbon) were analyzed on a scanning electron microscope (SEM) (JSM-5900LV, JEOL, Japan) and a transmission electron microscope (TEM) (JEM-2100F, JEOL, Japan). The surface characteristics and structures of the solid powder (activated carbon) were analyzed on a nitrogen adsorption/desorption gas analyzer (Micromeritics, USA) and an X-ray diffraction (XRD) (D8, Bruker, USA), respectively.

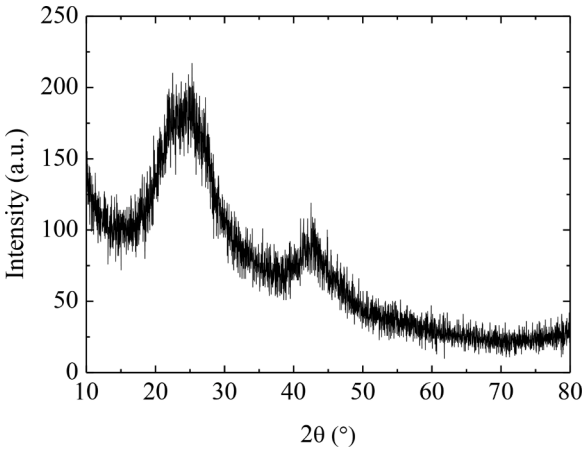

Fig. 1. XRD pattern of the solid powder.

A mixture consisting of the solid powder (activated carbon) and polyvinylidene fluoride (PVDF) (Kynar HSV 900, France) powder at a weight ratio of 9:1 was ground in an agate mortar for 30 min at room temperature. The ground mixture was placed in an oven at 80 °C for 1 h to improve the bonding between the PVDF powder and the solid powder. After the oven temperature was cooled to room temperature, the ground mixture of different masses was taken out of the oven and compressed in a Universal Tension Machine (ESA-CU200, Shimadzu, Japan) to form disks of ~8 mm in diameter under a load of 50 N. The mass of the disks was controlled in a range of 5 to 12.5 mg, which yielded the electrode disks with thickness in a range of 0.281 to 0.547 mm (0.281±0.010, 0.346±0.018, 0.441±0.002 and 0.547±0.002 mm). Symmetrical, two-electrode supercapacitors were assembled with the prepared disks as electrodes. The effects of compressive load and the mass loading (the electrode thickness) on the electrochemical performance, such as galvanostatic charge and discharge (GCD), cyclic voltammetry (CV), and electrochemical impedance spectroscopy (EIS), of the supercapacitors were characterized on an electrochemical workstation (PARSTAT MC, Princeton Applied Research, US). The compressive load was controlled in a range of 100 to 400 N. The tapping densities of the electrodes without the action of compressive stress were 0.344±0.025, 0.419±0.029, 0.439±0.021 and 0.442±0.021 mg/mm^3 for the mass loading of 5, 7.5, 10 and 12.5 mg, respectively, at compression-free state.

Note that there are different approaches used to construct the electrode materials for supercapacitors, including binder-free electrode [23], PTFE only [24], acetylene black (AB) agglomeration [25], etc. In this work, we only used PVDF as binder. The effects of other binders and AB will be studied in the future.

3. Results

Fig. 1 presents the XRD pattern of the solid powder after the physical activation. There are two broad peaks centered at 2θ = ~25.3° and ~42.5°, representing the reflections of (002) and (100) planes, respectively, from disordered carbon lattice. The broad peak centered at ~42.5° reveals the presence of weak crystallinity of the disordered carbon. This result suggests that the solid powder derived from the potato after the hydrothermal carbonization and H_2O-steam activation is disordered carbon, i.e. the consecutive hydrothermal carbonization and H_2O-steam activation of the potato mash indeed produced activated carbon.

Fig. 2a-b depicts SEM images of the potato-derived ACs. In contrast to the AC microspheres derived from xylose [20,26,27] and fructose [28-30], the potato-derived ACs exhibit a porous structure with solid

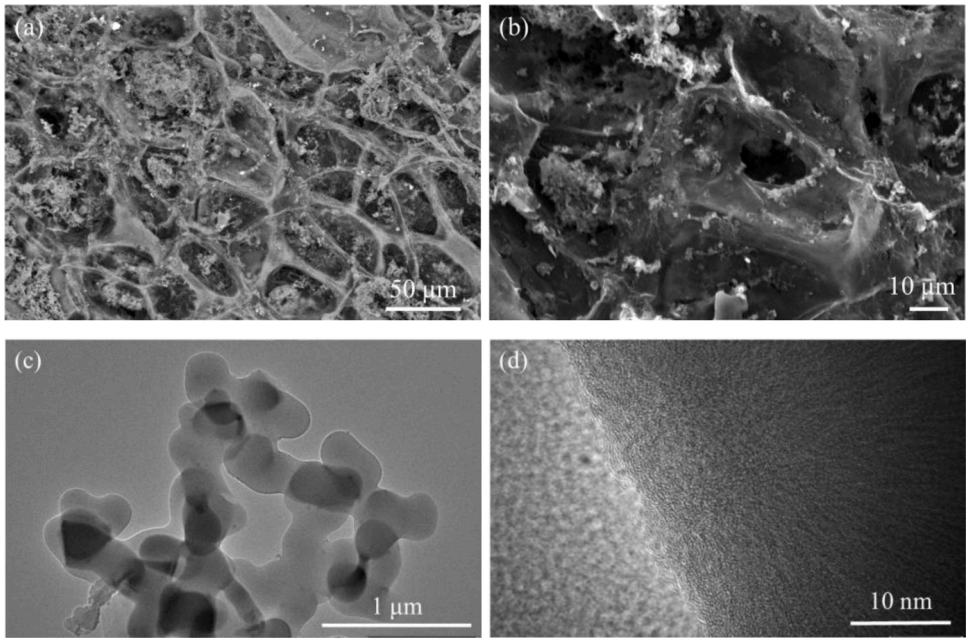

Fig. 2. (a)-(b) SEM images of the potato-derived ACs, (c) TEM image of the potato-derived AC, and (d) HRTEM image of the potato-derived AC.

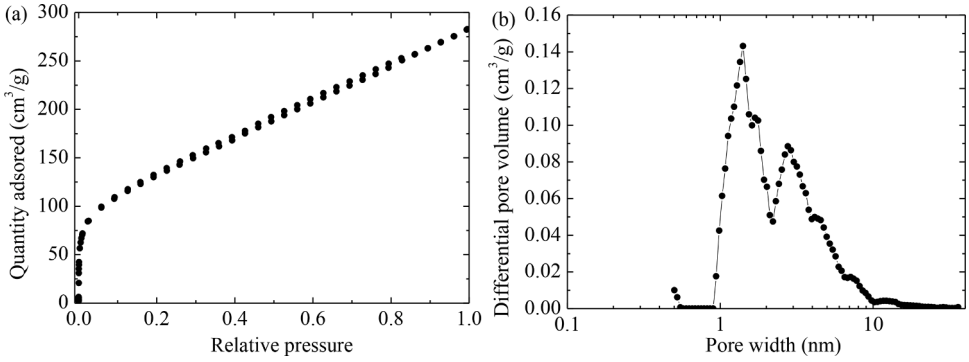

Fig. 3. (a) Nitrogen adsorption/desorption isotherms, and (b) distribution of pore widths.

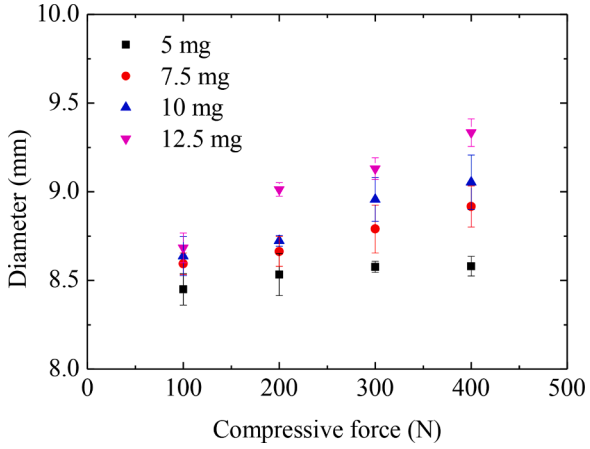

Fig. 4. Variation of the diameter of the electrode disks with compressive load after concurrent action of compressive load and electrochemical cycling.

"ligaments" of 10–15 μm in diameter and pores of 10–50 μm in size. The TEM image in Fig. 2c reveals the presence of pores of submicron meter in size and interconnected "ligaments" of submicron meter in size. That is to say, the porous ACs are a hierarchical structure with a two-level network, which possesses solid "ligaments" of two different length scales. No lattice fringe is observed from the HRTEM (high-resolution TEM) image in Fig. 2d, confirming the disordered structure of the potato-derived ACs. Such a result is consistent with the XRD pattern shown in Fig. 1.

The nitrogen adsorption/desorption isotherms of the potato-derived ACs is shown in Fig. 3a. The nitrogen adsorption/desorption isotherms exhibit type II characteristic, suggesting the presence of micropores and mesopores. The hysteresis loop can be attributed to the irreversible uptake of nitrogen in a portion of pores, whose pore width is approximately the same as the nitrogen molecules, and/or to the adsorption-induced swelling of the compliant structure of porous ACs [31].

From the nitrogen adsorption/desorption isotherms, we obtained the distribution of the pore width of the porous ACs (Fig. 3b). It is evident that the pore width spans from 0.94 nm to ~15 nm. The first peak is centered at ~1.41 nm, and the second peak is centered at ~2.77 nm. The porous ACs consist of micropores and mesopores.

Fig. 4 depicts the diameter of the electrode disks after concurrent action of compressive load and electrochemical cycling. It is evident that the diameter of the electrode disks increases with the increase of the compressive force for the electrode disks with mass larger than or equal to 7.5 mg. Such a trend reveals the compression-induced radial displacement of the electrode materials. For the electrode disks of 5 mg

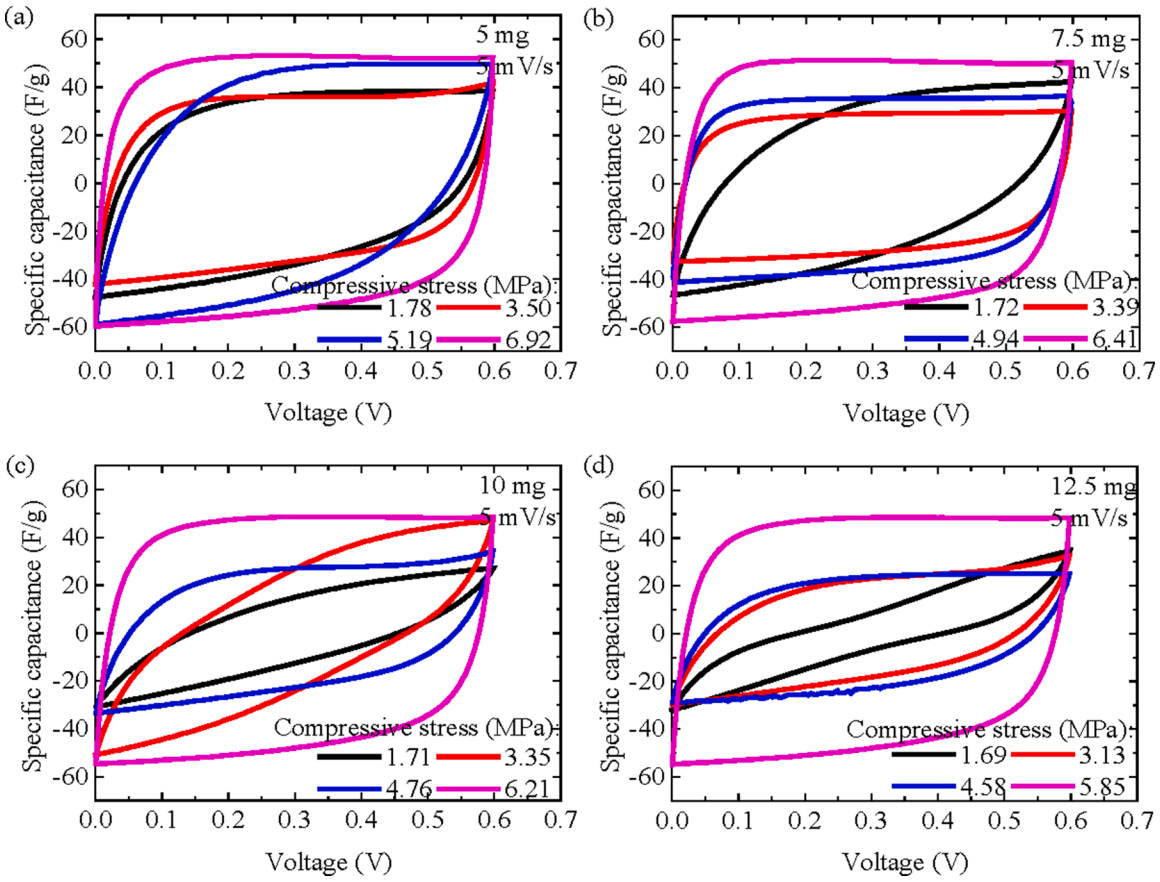

Fig. 5. CV curves of the supercapacitors at a scan rate of 5 mV/s with a voltage window in a range of 0 to 0.6 V under different compressive stresses for different electrode masses: (a) 5 mg, (b) 7.5 mg, (c) 10 mg and (d) 12.5 mg.

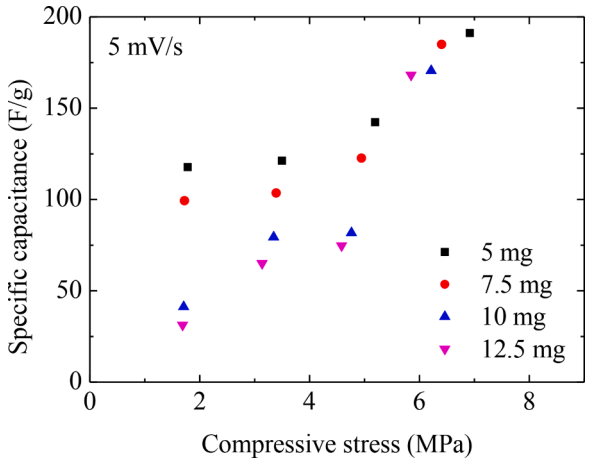

Fig. 6. Variation of the specific-gravimetric capacitance of the supercapacitors with compressive stress, as calculated from the CV curves.

in mass, the diameter of the electrode disks increases first with the increase of the compressive load and reaches plateau for the compressive force larger than or equal to 200 N. Such behavior suggests the limited effect of the compressive force on the deformation in radial direction for the electrode disks with thickness less than ~0.2 mm.

Using the diameters of the electrode disks, shown in Fig. 4, after the concurrent action of compressive load and electrochemical cycling, we calculated the compressive stresses applied to the supercapacitors. Fig. 5 depicts the CV curves of the supercapacitors with different electrode masses at a scan rate of 5 mV/s under different compressive stresses. For the supercapacitors with the electrode mass of 5 mg, all the CV curves are presented in a quasi-rectangular shape. For the supercapacitors with the electrode mass larger than or equal to 7.5 mg, the CV curves under the compressive stress of 1.69, 1.71 and 1.72 MPa are presented in a slender shape. Increasing compressive stress improves the capacitive characteristic of the supercapacitors and the energy storage in the supercapacitors.

Using the CV curves, we calculated the specific-gravimetric capacitance of the supercapacitors. Fig. 6 shows the variation of the specific-gravimetric capacitance of the supercapacitors with compressive stress for a scan rate of 5 mV/s. It is evident that the specific-gravimetric capacitance of the supercapacitors is dependent on the mass loading of the electrode material and the magnitude of compressive stress. For the electrode of the same mass loading, increasing compressive stress increases the specific capacitance. However, there exist an upper limit of the compressive stress, which is determined by the mechanical properties of the separator, and an upper limit of specific capacitance, which is determined by the compaction density of the electrode material. For the same compressive stress with a magnitude less than or equal to 5.19 MPa, the specific-gravimetric capacitance of the supercapacitors increases with the decrease of the mass loading of the electrode.

Fig. 7 shows the GCD curves of the supercapacitors of different electrode masses at a current density of 1 A/g under different compressive stresses. It is evident that both the charging and discharging times increases with the increase of compressive stress for the same electrode mass. For the same compressive stress, increasing the electrode mass leads to the decrease of both the charging and discharging times. Also, increasing compressive stress results in the decrease of the IR drop, suggesting the decrease of the contact resistance between the electrode materials and the current collectors and between the porous

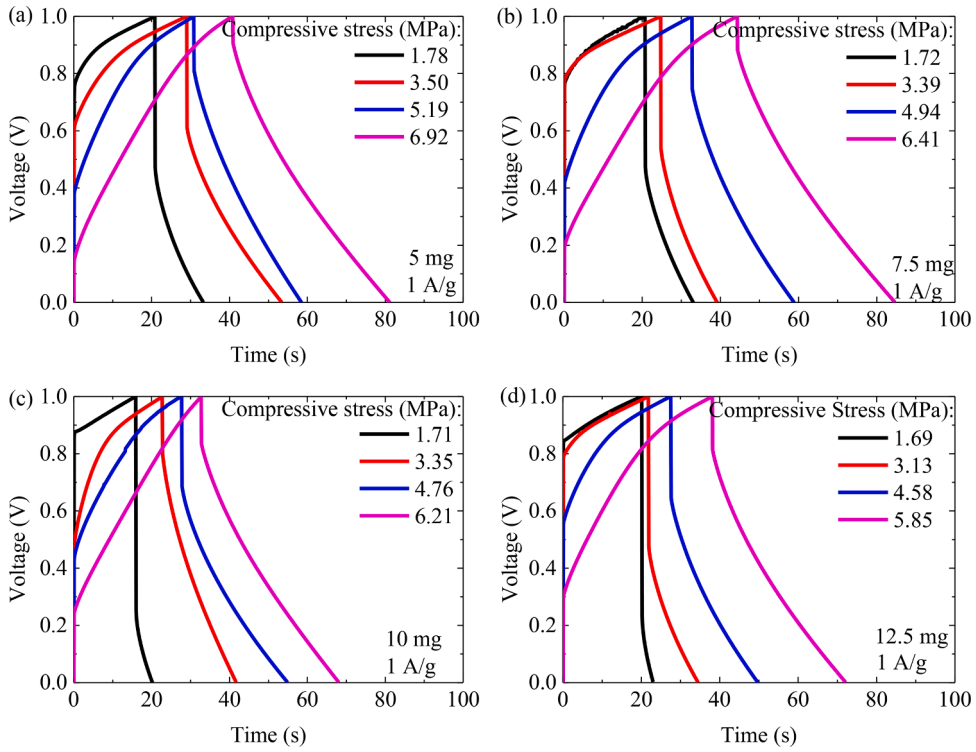

Fig. 7. GCD curves of the supercapacitors at a current density of 1 A/g under different compressive stresses for different electrode masses: (a) 5 mg, (b) 7.5 mg, (c) 10 mg, and (d) 12.5 mg.

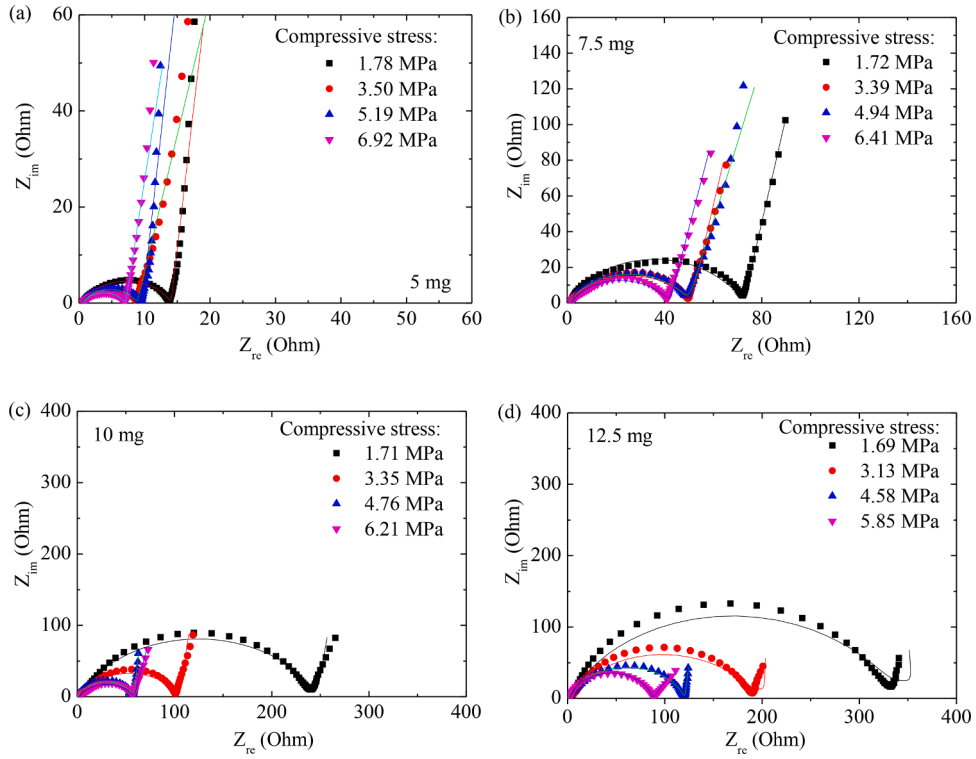

Fig. 8. Nyquist plots of the supercapacitors under different compressive stresses for different electrode masses: (a) 5 mg, (b) 7.5 mg, (c) 10 mg and (d) 12.5 mg.

ACs.

Fig. 8 presents the Nyquist plots of the supercapacitors with different electrode masses in a frequency range of 1 mHz to 1 MHz under different compressive stresses. There are a circular segment in the regime of high frequency and a nearly vertical, straight segment in the regime of low frequency. There is a small, non-vertical segment between the regime of high frequency and the regime of low frequency, as shown in Fig. 8a, which corresponds to the regime of intermediate frequency and is associated with ionic migration in the supercapacitors. From Fig. 8, we note that the compressive stress applied to the supercapacitors has no

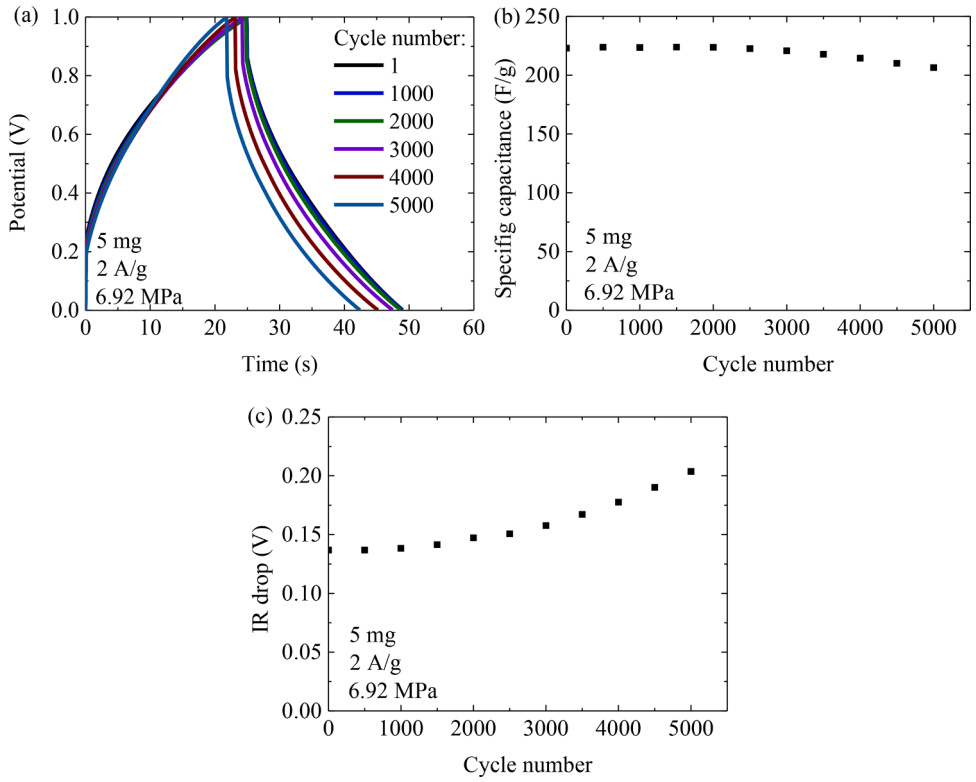

Fig. 9. Long-term performance of the supercapacitors at the current density of 2 A/g under 6.92 MPa for the electrode mass of 5 mg: (a) GCD curves, (b) specific-gravimetric capacitance, and (c) IR drop.

significant effect on the series resistance, as determined by the left intercept of the Nyquist plot with the Z_{re}-axis. However, the intrinsic resistance of the supercapacitors generally decreases with the increase of the compressive stress. This behavior is due to that the intrinsic resistance consists of the contribution of the contact resistance between adjacent ACs, which is inversely proportional to the contact area for Ohmic resistance. Increasing compressive stress increases the contact area between adjacent ACs, leading to the decrease of the contact resistance and the intrinsic resistance.

According to Figs. 6-8, we can conclude that the supercapacitors with 5 mg per electrode exhibited the best electrochemical performance under the largest compressive stress of 6.92 MPa. The long-term performance of the supercapacitors with 5 mg per electrode under 6.92 MPa was examined. Fig. 9a depicts the GCD curves of the supercapacitors with 5 mg per electrode at different instants at a current density of 2 A/g under the compressive stress of 6.92 MPa. From the GCD curve (Fig. 9a), we calculated the specific-gravimetric capacitance and IR drop at different instants. Fig. 9b shows the variation of the specific-gravimetric capacitance with the cycle number, as expected. The specific-gravimetric capacitance decreases slowly from an initial value of 223.0 F/g to the value of ~206.4 F/g aft the 5000-th cycle. There is ~7.4% decrease in the specific-gravimetric capacitance after the 5000-th cycle. Concurrently, the IR drop increases slowly with the increase of the cycle number from 0.137 V to 0.204 V (Fig. 9c), leading to the increase in the energy loss. The increase of the IR drop with the increase of the cycle number is likely due to the interpenetration of glycerol and the water in the aqueous KOH electrolyte, resulting in the increase of the resistance to ionic migration in the electrode. Note that the edge of the prepared supercapacitors was covered by glycerol; such a design allows for the calculation of the compressive stress applying on the supercapacitor.

4. Discussion

Sun et al. [20] assumed that there is no significant change in the diameter of the electrode disks of 0.1 mm in thickness in their study of the effect of compressive stress on the electrochemical performance of the supercapacitors with xylose-derived AC spheres as electrode material and Na_2SO_4 aqueous solution as electrolyte. Such an approximation is likely reasonable for the electrode disks of 0.1 mm in thickness, as supported by the results for the compression of the electrode disks of 0.281 mm in thickness in Fig. 4. However, there are finite changes in the diameters of the electrode disks with the disk thicknesses in a range of 0.281 to 0.547 mm, as revealed in Fig. 4. Thus, the effect of the diameter change of the electrode disks on the stress dependence of the electrochemical performance of the supercapacitors needs to be considered in the analysis.

Here, we used a different approach to analyze the compression effect on the specific capacitance of the supercapacitors from that given by Sun et al. [20]. Under the action of mechanical stress, the adsorption in a porous AC as a function of volumetric strain, ε_V, can be expressed as [32]

$$n(\varepsilon_V) = n_0(1 + \lambda\varepsilon_V) \tag{1}$$

where n_0 and n are the amount of the material (gas) adsorbed in the porous AC at strain-free and deformation states, respectively, and λ is the coupling parameter representing the mechanosorptive effect. In general, the specific surface area, S, of the porous AC is proportional to the amount of the material (gas) adsorbed in the pores of the porous AC, i.e. $S \propto n_V$. There is

$$S = S_0(1 + \lambda\varepsilon_V) \tag{2}$$

with S_0 being the specific surface area of the porous AC at the strain-free state.

There are two aspects contributing to the charge storage in supercapacitor – one is the surface area and the other is the interaction

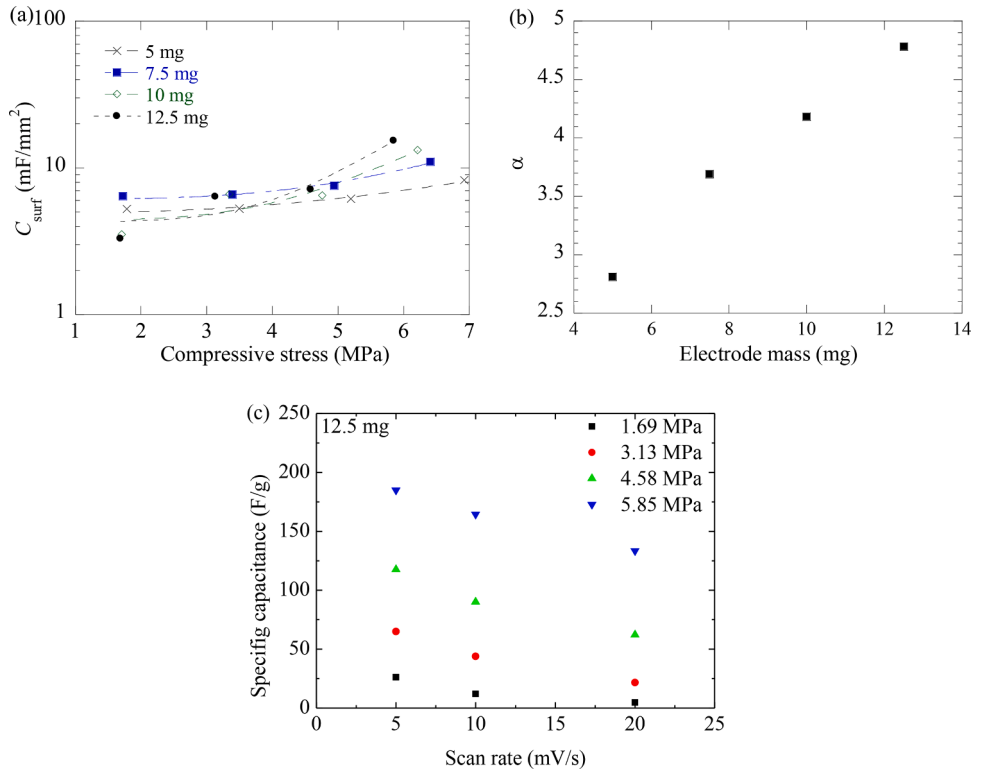

Fig. 10. (a) Variation of the specific-areal capacitance of the supercapacitors with the compressive stress at a scan rate of 5 mV/s under different compressive stresses, (b) variation of α with the electrode mass, and (c) rate dependence of the specific-gravimetric capacitance of the supercapacitors with the mass loading of 12.5 mg under different compressive stresses.

between ions and the surface of the active material. Increasing surface area increases the sites available for the accumulation of ions on the surface of the active material, leading to the increase in the energy storage in supercapacitors, as reported in literature [33-35]. Recently, Zhou and Yang [36] derived analytical expression for the integral capacitance of a rectangular structure and demonstrated that the integral capacitance of a rectangular structure of the same cavity area/volume increase with the increase of the surface area.

According to the result given by Sun et al. [37], the specific-areal capacitance, C_{surf}, of an AC-based supercapacitor is proportional to the specific surface area of the porous AC. Thus, there is

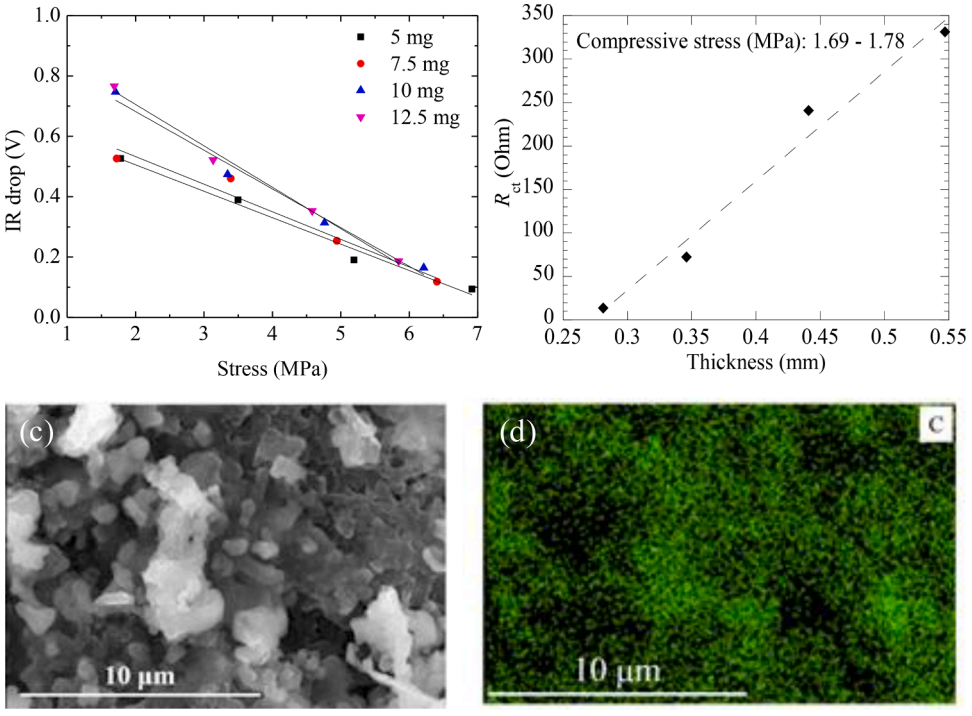

Fig. 11. (a) Variation of the IR drop of the supercapacitors with the compressive stress at a current density of 1 A/g for the electrodes with different mass loading, (b) variation of the intrinsic resistance, R_{ct}, with the electrode thickness for the smallest compressive load of 100 N with the corresponding stress in a range of 1.69 – 1.78 MPa at a current density of 1 A/g, (c) SEM image of an electrode disk from potato-derived ACs with a mass loading of 12.5 mg, and (d) EDS map of carbon over the area corresponding to figure c.

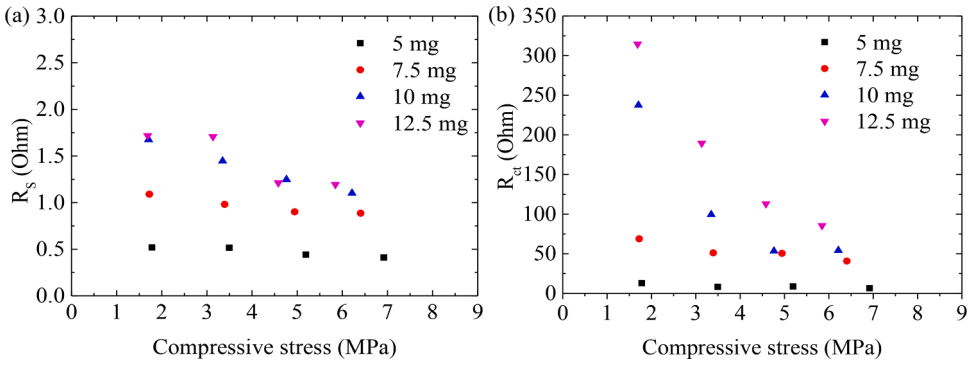

Fig. 12. Variation of the series resistance and the intrinsic resistance with the compressive stress for the supercapacitors with the electrodes of different masses: (a) R_s, and (b) R_{ct}.

$$C_{surf} = C_0(1 + \lambda\varepsilon_V) \tag{3}$$

with C_0 being the specific areal capacitance of the AC-based supercapacitor at the strain-free state. For thin-layer porous materials under uniaxial compression, the compressive strain is generally proportional to the volumetric strain. Thus, there is a power-law correlation between the compressive stress, σ, and the volumetric strain as

$$\varepsilon_V = k\sigma^{\alpha} \tag{4}$$

with k as a constant and α as a power index. Substituting Eq. (4) in (3) yields

$$C_{surf} = C_0(1 + \chi\sigma^{\alpha}) \tag{5}$$

where χ ($= k\lambda$) is a constant, depending on the mechanosorptive effect and the correlation between the volumetric strain and the compressive stress.

Fig. 10a shows the variation of the specific-areal capacitance of the supercapacitors with the compressive stress, in which the capacitance was calculated from the CV curves. It is evident that the specific-areal capacitance increases with the increase of the compressive stress, suggesting that applying compressive stress increases the energy storage in the supercapacitors with the potato-derived ACs as the electrode materials. Using Eq. (5) to curve-fit the data in Fig. 10a, we obtained the numerical values of the power index of α. Fig. 10b displays the variation of the power index of α with the mass loading of the electrode disks. The power index of α increases with the increases of the mass loading. Such an increasing trend in the power index of α suggests the dependence of the degree of compaction of the electrode disks on the compressive stress and the disk thickness.

Fig. 10c presents the rate dependence of the specific-gravimetric capacitance of the supercapacitors with the mass loading of 12.5 mg under different compressive stresses. It is evident that the compressive stress has little effect on the rate performance of the supercapacitors.

Fig. 11a shows the variation of the IR drop of the supercapacitors with the compressive stress at a current density of 1 A/g for the electrodes with different mass loading. It is evident that the IR drop is a linearly decreasing function of the compressive stress as

$$IR = IR_0 - a\sigma \tag{6}$$

where IR_0 and IR are the IR drops at the stress-free and deformation states, respectively, and a is a constant representing the decreasing rate of the IR drop per unit stress. Using Eq. (6) to fit the data in Fig. 11a, we obtained (IR_0, a) in the units of (V, V/MPa) as (0.68, 0.088), (0.72, 0.091), (0.94, 0.13) and (0.98, 0.14) for the electrode disks with the mass loading of 5, 7.5, 10 and 12.5 mg, respectively. It is evident that the IR drop at the stress-free state is an increasing function of the disk thickness (mass loading) and the decreasing rate of the IR drop per unit stress, a, also increases with the increase of the disk thickness (mass loading). Such trends can be attributed to that a thicker electrode disk is more compliant than a thinner one and more contacts between nearby porous ACs can occur to reduce the resistance under the same compressive stress.

The internal resistance calculated from the IR drop is in a range of 10 – 52 Ohm. The reason for such "large" internal resistance is unclear. It might be due to the cavities of micron sizes, as shown in Fig. 2a, and there are also contributions from the electrical double-layer structures. To decrease the internal resistance, one can add conducting materials, such as AB, to increase electrical conduction.

From the Nyquist plot of Fig. 8, we calculated the series resistance, R_s, and the intrinsic resistance, R_{ct}, consisting of interfacial resistance, contact resistance, charge transfer resistance and resistance to ionic migration, from the left and right intersections of the Nyquist plot with the Z_{re} axis of the Nyquist plot, respectively. Fig. 11b presents the variation of the intrinsic resistance, R_{ct}, with the electrode thickness for the smallest compressive load of 100 N with the corresponding stresses in a range of 1.69 – 1.78 MPa at a current density of 1 A/g. It is evident that the intrinsic resistance is an approximately linearly increasing function of the electrode thickness. Such behavior suggests the Ohmic-like characteristic of the intrinsic resistance.

Fig. 12a-b illustrates the variations of R_s and R_{ct} with the compressive stress for the supercapacitors with the electrodes of different masses. Both the series resistance and the intrinsic resistance decrease with the increase of the compressive stress, which is in consistence with the decreasing trend of the IR drop with the increase of the compressive stress. Applying compressive stress not only increases the contact sizes between adjacent porous ACs through local deformation but also causes the rearrangement of the porous ACs, which leads to the decrease of the energy loss during electrochemical cycling. Note that there are large drops in the intrinsic resistance for the supercapacitors with thick electrodes under the action of the compressive stress, which suggests much nonuniform structures presented in the thick electrodes. As shown in Fig. 11c, there are significant numbers of AC-PTFE aggregates of different sizes and cavities in the electrode and the aggregates distribute heterogeneously. Fig. 11d shows the EDS map of carbon over the area corresponding to Fig. 11c. It is evident that carbon distributes nonuniformly.

According to Vicentini et al. [38], the resistance calculated from the IR drop is "equivalent" to R_s instead of R_{ct}. From Figs. 11a and 12a, we note that the resistance calculated from the IR drop is about one to two orders of the corresponding value of R_s. Such a difference is likely due to the frequency dependence of the electric resistivity of the systems, including the porous structure [39] and ionic conductivity of an aqueous solution [40]. According to the results given by Revil [39] and Chandra and Bagchi [40], the electrical conductivity of porous materials with aqueous electrolyte increases with the increase of frequency, i.e. the electric resistivity at a lower frequency is larger than that at a higher frequency. The experimental results exhibit similar trend to the analysis

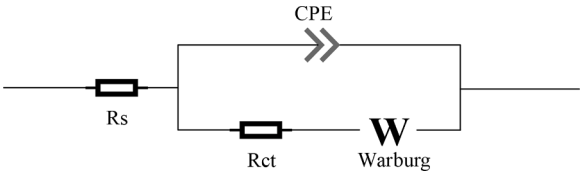

Fig. 13. Schematic of the equivalent circuit for the supercapacitors.

given by Revil [39].

To analyze the ionic diffusion in the supercapacitors during electrochemical cycling, a lumped-element circuit (Fig. 13) was used to fit the Nyquist plot of Fig. 8. The fitting curves are included in Fig. 8. It is evident that the lumped-element circuit describes relatively well the behavior of the supercapacitors under a small amplitude, alternating current. The confidence for the curve fitting is larger than 0.92 for all the fitting, even though the fitting results aren't perfect for the thickest electrode under small compressive stresses (Fig. 8d).

The Warburg impedance of finite-space diffusion, Z_ω, which was used to represent the Warburg element in the circuit, as a function of angular frequency, ω, is

$$Z_\omega = \frac{\sigma_\omega}{\sqrt{2\omega}}(1-i)\coth\left(W_{oc}\sqrt{i\omega}\right) \text{ with } W_{oc} = \frac{d}{\sqrt{D}} \tag{7}$$

where σ_ω is the Warburg coefficient, d is the diffusion thickness, and D is the diffusion coefficient. From the Warburg coefficient, we can calculate the diffusion coefficient as [41]

$$D = \frac{R_g^2 T^2}{2A^2 n_i^4 F^4 C_i^2 \sigma_\omega^2} \tag{8}$$

where R_g is the gas constant, T is absolute temperature, A is the area per electrode, n_i is the charge number of electrolyte ions, F is the Faraday constant, and C_i is the concentration of electrolyte.

Fig. 14a depicts the variation of the Warburg coefficient with the compressive stress for the supercapacitors with the electrodes of different masses. It is evident that the Warburg coefficient decreases with the increase of the compressive stress. However, the applied compressive stress has a limited effect on the Warburg coefficient for the electrodes with 5 mg in mass.

Using Eq. (8) and the Warburg coefficient in Fig. 14a, we calculated the diffusion coefficient for the ionic diffusion in the supercapacitors. The diffusion coefficient for the supercapacitors with the electrodes of the same mass exhibits a slightly increasing trend with the increase of the compressive stress. The larger the compressive stress, the larger is the diffusion coefficient. The diffusion coefficient for the supercapacitors with the electrodes of 5 mg in the mass loading is largest under the same compressive stress. There is no significant difference in the diffusion coefficient for the supercapacitors with the electrodes of the mass loading in the range of 7.5 to 12.5 mg under the action of the same compressive stress.

Table 1 lists the specific-gravimetric capacitances of some supercapacitors under the action of mechanical loading, which are available in literature. It is evident that the specific-gravimetric capacitances obtained in this work are larger than most results reported in literature. Applying compressive stress is a feasible approach to improve the electrochemical performance of AC-based supercapacitors.

5. Summary

Considering the potential applications of biomass-derived ACs in the energy storage, we have studied the electrochemical characteristics of the symmetrical, two-electrode supercapacitors with the potato-derived porous ACs as electrode materials under the concurrent action of compressive stress. Applying compressive stress causes the compaction of the potato-derived porous ACs and reduces the migration distance of ions to the surfaces of the potato-derived porous ACs, which results in the decrease of both the series and intrinsic resistances. The experimental results show that the potato-derived supercapacitors exhibit higher specific-gravimetric capacitance than most results reported in literature and the specific-areal capacitance increases with the increase of the compressive stress in a power-law formulation. The calculated diffusion coefficient for ionic migration in the electrodes of the same mass exhibits a slightly increasing trend with the increase of the compressive stress.

Table 1
Specific-gravimetric capacitances of some supercapacitors under the action of mechanical loading.

Material	Stress kPa	Specific capacitance F/g	Electrolyte	Concentration M
Green monoliths [13]	14.3~23.8	5~30	H_2SO_4	1
Activated carbon fabric [19]	414~2068	10~110	KCl	1
Activated carbon fabric [19]	414~2068	15~120	LiCl	1
Activated carbon fabric [19]	414~2068	5~80	KNO_3	1
Xylose [20]	2550~40,570	133~238	Na_2SO_4	1
Xylose [20]	2550~40,570	122~202	Na_2SO_4	0.75
Xylose [20]	2550~40,570	115~187	Na_2SO_4	0.5
Xylose [20]	2550~40,570	110~159	Na_2SO_4	0.25
Potato (this work)	1689~6918	117.6~223.0	KOH	6

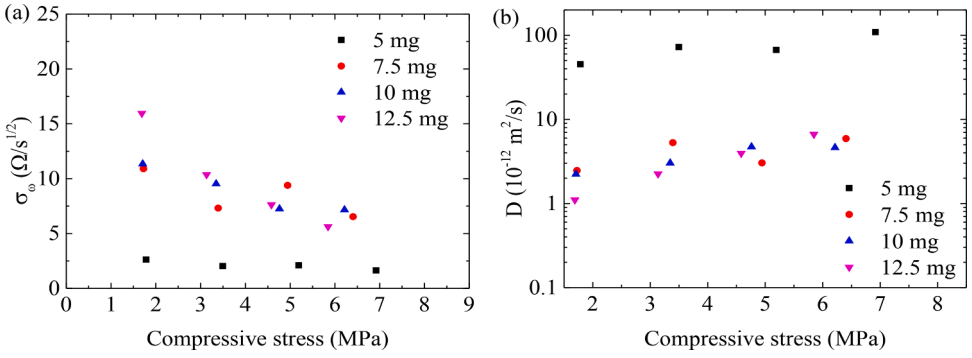

Fig. 14. Variations of the Warburg coefficient and diffusion coefficient with compressive stress for the supercapacitors with electrodes of different masses: (a) σ_ω, and (b) D.

The experimental results reveal that increasing the compaction of the electrode materials by applying compressive stress can increase the energy storage in supercapacitors. The approach developed in this work opens a potential route to increase the performance and structural integrity of supercapacitors and a method to investigate the stress effects on the ACs-based supercapacitors from different biomasses, including YP-50, with similar surface characteristics.

Credit author statement

YZ: Experimental design, Electrochemical characterization, Data curation, Writing.

WS: Materials Characterization and Sample preparation.

FY: Conceptualization, Methodology, Writing- Editing.

Declaration of Competing Interest

The authors declare that they have no known competing financial interests or personal relationships that could have appeared to influence the work reported in this paper.

Acknowledgments

FY is grateful for the support from the NSF (CMMI-1634540), monitored by Dr. Khershed Cooper. WS is grateful for the support from the National Natural Science Foundation of China (No. 21805123).

References

[1] P. Xu, T. Gu, Z. Cao, B. Wei, J. Yu, F. Li, J.-.H. Byun, W. Lu, Q. Li, T.-.W. Chou, Carbon nanotube fiber based stretchable wire-shaped supercapacitors, Adv. Energy Mater. 4 (2014), 1300759.
[2] Q. Tang, W. Wang, G. Wang, Alkali-resistant quasi-solid-state electrolyte for stretchable supercapacitors, ACS Appl. Mater. Interfaces 8 (2016) 27701–27709.
[3] D. Shin, C. Shen, M. Sanghadasa, L. Lin, Breathable 3D supercapacitors based on activated carbon fiber veil, Adv. Mater. Technol. 3 (2018), 1800209.
[4] H. Luo, H. Lu, J. Qiu, Carbon fibers surface-grown with helical carbon nanotubes and polyaniline for high-performance electrode materials and flexible supercapacitors, J. Electroanal. Chem. 828 (2018) 24–32.
[5] J.-H. Liu, X.-Y. Xu, W. Lu, X. Xiong, X. Ouyang, C. Zhao, F. Wang, S.-Y. Qin, J.-L. Hong, J.-N. Tang, D.-Z. Chen, A high performance all-solid-state flexible supercapacitor based on carbon nanotube fiber/carbon nanotubes/polyaniline with a double core-sheathed structure, Electrochim. Acta 283 (2018) 366–373.
[6] Y. Wang, B. Liu, Q. Li, S. Cartmell, S. Ferrara, Z.D. Deng, J. Xiao, Lithium and lithium ion batteries for applications in microelectronic devices: a review, J. Power Sources 286 (2015) 330–345.
[7] G. Zubi, R. Dufo-López, M. Carvalho, G. Pasaoglu, The lithium-ion battery: state of the art and future perspectives, Renew. Sustain. Energy Rev. 89 (2018) 292–308.
[8] J. Li, X. Yun, Z. Hu, L. Xi, N. Li, H. Tang, P. Lu, Y. Zhu, Three-dimensional nitrogen and phosphorus co-doped carbon quantum dots/reduced graphene oxide composite aerogels with a hierarchical porous structure as superior electrode materials for supercapacitors, J. Mater. Chem. A 7 (2019) 26311–26325.
[9] Y. Zhu, Z. Huang, Z. Hu, L. Xi, X. Ji, Y. Liu, 3D interconnected ultrathin cobalt selenide nanosheets as cathode materials for hybrid supercapacitors, Electrochim. Acta 269 (2018) 30–37.
[10] L. Dong, C. Xu, Y. Li, Z.-.H. Huang, F. Kang, Q.-.H. Yang, X. Zhao, Flexible electrodes and supercapacitors for wearable energy storage: a review by category, J. Mater. Chem. A 4 (2016) 4659–4685.
[11] Y. Bu, T. Sun, Y. Cai, L. Du, O. Zhuo, L. Yang, Q. Wu, X. Wang, Z. Hu, Compressing carbon nanocages by capillarity for optimizing porous structures toward ultrahigh-volumetric-performance supercapacitors, Adv. Mater. 29 (2017), 1700470.
[12] X. Li, T. Gu, B. Wei, Dynamic and galvanic stability of stretchable supercapacitors, Nano Lett. 12 (2012) 6366–6371.
[13] A. Awitdrus, M. Deraman, I.A. Talib, R. Farma, R. Omar, M.M. Ishak, N.H. Basri, B. N.M. Dolah, Effect of compression pressure on the physical and electrochemical properties of activated carbon monoliths electrodes for supercapacitor application, Adv. Mater. Res. 501 (2012) 13–18.
[14] X. Li, J. Rong, B. Wei, Electrochemical behavior of single-walled carbon nanotube supercapacitors under compressive stress, ACS Nano 4 (2010) 6039–6049.
[15] Y. Zhao, J. Liu, Y. Hu, H. Cheng, C. Hu, C. Jiang, L. Jiang, A. Cao, L. Qu, Highly compression-tolerant supercapacitor based on polypyrrole-mediated graphene foam electrodes, Adv. Mater. 25 (2013) 591–595.
[16] P. Li, C. Kong, Y. Shang, E. Shi, Y. Yu, W. Qian, F. Wei, J. Wei, K. Wang, H. Zhu, A. Cao, D. Wu, Highly deformation-tolerant carbon nanotube sponges as supercapacitor electrodes, Nanoscale 5 (2013) 8472–8479.
[17] Y. Chen, K. Cai, C. Liu, H. Song, X. Yang, High-performance and breathable polypyrrole coated air-laid paper for flexible all-solid-state supercapacitors, Adv. Energy Mater. 7 (2017), 1701247.
[18] X. Zhang, J. Zhao, X. He, Q. Li, C. Ao, T. Xia, W. Zhang, C. Lu, Y. Deng, Mechanically robust and highly compressible electrochemical supercapacitors from nitrogen-doped carbon aerogels, Carbon N Y 127 (2018) 236–244.
[19] C. Masarapu, L.-P. Wang, X. Li, B. Wei, Tailoring electrode/electrolyte interfacial properties in flexible supercapacitors by applying pressure, Adv. Energy Mater. 2 (2012) 546–552.
[20] W. Sun, Y. Zhang, F. Yang, Tuning electrochemical performance of carbon-sphere-based supercapacitors by compressive stress, Electrochim. Acta 357 (2020), 136874.
[21] S. Liang, A.G. McDonald, Chemical and thermal characterization of potato peel waste and its fermentation residue as potential resources for biofuel and bioproducts production, J. Agric. Food Chem. 62 (2014) 8421–8429.
[22] D. Bose, Potentials of Potato Starch For Biofuel production. Fermentative Production of Alcohol By Saccharomyces Cerevisiae Utilizing Potato Starch, GRIN Verlag, 2016.
[23] L. Fan, L. Yang, X. Ni, J. Han, R. Guo, C.J. Zhang, Nitrogen-enriched meso-macroporous carbon fiber network as a binder-free flexible electrode for supercapacitors, Carbon N Y 107 (2016) 629–637.
[24] Z. Zhu, S. Tang, J. Yuan, X. Qin, Y. Deng, R. Qu, G.M. Haarberg, Effects of various binders on supercapacitor performances, Int. J. Electrochem. Sci. 11 (2016) 8270–8279.
[25] H. Zhang, W. Zhang, J. Cheng, G. Cao, Y. Yang, Acetylene black agglomeration in activated carbon based electrochemical double layer capacitor electrodes, Solid State Ion. 179 (2008) 1946–1950.
[26] F.-C. Huang, C.-K. Lee, Y.-L. Han, W.-C. Chao, H.-.P. Chao, Preparation of activated carbon using micro-nano carbon spheres through chemical activation, J. Taiwan Inst. Chem. Eng. 45 (2014) 2805–2812.
[27] P. Waribam, S.D. Ngo, T.T.V. Tran, S. Kongparakul, P. Reubroycharoen, N. Chanlek, L. Wei, H. Zhang, G. Guan, C. Samart, Waste biomass valorization through production of xylose-based porous carbon microspheres for supercapacitor applications, Waste Manag. 105 (2020) 492–500.
[28] W. Cao, F. Yang, Supercapacitors from high fructose corn syrup-derived activated carbons, Mater. Today Energy 9 (2018) 406–415.
[29] H. Zhao, X. Lu, Y. Wang, B. Sun, X. Wu, H. Lu, Effects of additives on sucrose-derived activated carbon microspheres synthesized by hydrothermal carbonization, J. Mater. Sci. 52 (2017) 10787–10799.
[30] Y. Zhong, Q. Lu, Y. Zhu, Y. Zhu, W. Zhou, S. Wang, Z. Shao, Fructose-derived hollow carbon nanospheres with ultrathin and ordered mesoporous shells as cathodes in lithium–sulfur batteries for fast energy storage, Adv. Sustain. Syst. 1 (2017), 1700081.
[31] A.M. Silvestre-Albero, J.M. Juárez-Galán, J. Silvestre-Albero, F. Rodríguez-Reinoso, Low-pressure hysteresis in adsorption: an artifact? J Phys Chem. C 116 (2012) 16652–16655.
[32] M. Bossert, A. Grosman, I. Trimaille, C. Nous, E. Rolley, Stress or strain does not impact sorption in stiff mesoporous materials, Langmuir 36 (2020) 11054–11060.
[33] T. Liu, F. Zhang, Y. Song, Y. Li, Revitalizing carbon supercapacitor electrodes with hierarchical porous structures, J. Mater. Chem. A 5 (2017) 17705–17733.
[34] A.J. Roberts, R.C. Slade, Effect of specific surface area on capacitance in asymmetric carbon/α-MnO_2 supercapacitors, Electrochim. Acta 55 (2010) 7460–7469.
[35] E. Taer, A. Agustino, R. Farma, R. Taslim, M. Paiszal, A. Ira, S. Yardi, Y. Sari, H. Yusra, S. Nurjanah, The relationship of surface area to cell capacitance for monolith carbon electrode from biomass materials for supercapacitor aplication, J. Phys.: Conf. Ser. 1116 (2018), 032040.
[36] W. Zhou, F. Yang, Integral capacitance of diffusion layer for rectangular structures, J. Energy Storage 30 (2020), 101477.
[37] W. Sun, S.M. Lipka, C. Swartz, D. Williams, F. Yang, Hemp-derived activated carbons for supercapacitors, Carbon N Y 103 (2016) 181–192.
[38] R. Vicentini, L.M. Da Silva, E.P. Cecilio Junior, T.A. Alves, W.G. Nunes, H. Zanin, How to measure and calculate equivalent series resistance of electric double-layer capacitors, Molecules 24 (2019) 1452.
[39] A. Revil, Effective conductivity and permittivity of unsaturated porous materials in the frequency range 1 mHz–1 GHz, Water Resour. Res. 49 (2013) 306–327.
[40] A. Chandra, B. Bagchi, Frequency dependence of ionic conductivity of electrolyte solutions, J. Chem. Phys. 112 (2000) 1876–1886.
[41] R. Vedalakshmi, V. Saraswathy, H.-W. Song, N. Palaniswamy, Determination of diffusion coefficient of chloride in concrete using Warburg diffusion coefficient, Corros. Sci. 51 (2009) 1299–1307.